J Mater Sci (2011) 46:2058–2063
DOI 10.1007/s10853-010-5038-7

Functionalization of electrospun magnetically separable TiO_2-coated $SrFe_{12}O_{19}$ nanofibers: strongly effective photocatalyst and magnetic separation

Cong-Ju Li · Jiao-Na Wang · Xiu-Yan Li · Lian-Lian Zhang

Received: 25 July 2010 / Accepted: 28 October 2010 / Published online: 17 November 2010

Abstract Magnetically separable TiO_2-coated $SrFe_{12}O_{19}$ electrospun nanofibers were obtained successfully by means of sol–gel, electrospinning, and coating technology, followed by heat treatment at 550–650 °C for 3 h. The average diameter of the electrospun fibers was 500–600 nm. The fibers were characterized by X-ray diffraction (XRD), scanning electron microscopy (SEM), transmission electron microscope (TEM), and vibrating sample magnetometer (VSM). The optimized calcining temperature was determined by XRD and the analysis of decolorizing efficiency of methylene blue (MB) under UV–vis irradiation. The photocatalytic activity of the TiO_2-coated $SrFe_{12}O_{19}$ fibers was investigated using ultraviolet–visible absorbance by following the photooxidative decomposition of a model pollutant dye solution, MB in a photochemical reactor. In contrast to pure TiO_2 fibers, the TiO_2-coated $SrFe_{12}O_{19}$ fibers have higher absorption in 250–750 nm wavelength regions. The presence of $SrFe_{12}O_{19}$ not only broadened the response region of visible-light, but also enhanced the absorbance for UV light. The decolorizing efficiency of MB under UV–vis irradiation was up to 98.19%, which was a little higher than that of Degussa P25 (97.68%). Furthermore, these fibers could be recollected easily with a magnet in a photocatalytic process and had effectively avoided secondary pollution of treated water.

C.-J. Li · J.-N. Wang · X.-Y. Li · L.-L. Zhang
College of Material Science and Engineering, Beijing Institute of Fashion Technology, Beijing 100029, China

C.-J. Li (✉) · J.-N. Wang · L.-L. Zhang
Beijing Key Laboratory of Clothing Materials R&D and Assessment, Beijing 100029, China
e-mail: congjuli@gmail.com

Introduction

Titania-mediated is useful as a chemical sensor, as a ceramic microporous membrane, as a catalyst and so on. It is especially well known for its remarkable photocatalytic properties. Titania photocatalyst has been extensively studied with regard to its application in removing organic pollutants from waste water for the past 20 years, and its photocatalytic oxidation and reduction offer potentially a facile and cheap method in environmental treatments [1–6].

In general, titania photocatalysts are in the form of either nanoparticles or thin films. Nanoparticles have a high active surface area but are difficult to recollect after use from the waste water. Moreover, under certain experimental conditions, nanoparticles have a strong tendency to agglomerate into larger particles, decreasing the photocatalytic activity [1, 7, 8]. Thin films are readily reused but have much less active surface areas than nanoparticles [7]. Therefore, some research groups have tried to prepare fibers to solve these problems [1, 3, 7, 9].

The electrospinning technique has been recognized as an effective, versatile, and mature method for the production of nanofibers with high surface-to-volume ratio and small diameters [1]. This technique was originally invented 70 years ago and has been used primarily for producing ultrathin polymer fibers [10–15]. In our previous study, magnetic inorganic nanofibers have been prepared by electrospinning combined with sol–gel technique [16, 17]. In order to recollect titania photocatalysts effectively, a novel coaxial fiber was prepared, where the M-type $SrFe_{12}O_{19}$ fiber was the core, and the TiO_2 coating was the sheath. There are three types of strontium ferrite: spinel-, garnet-, and magnetoplumbite-type (M-type) ferrite. Among them, M-type strontium ferrite belongs to hexagonal crystal system, and it

offers several kinds of non-equivalent sites, octahedral, bipyramidal, and tetrahedral, which can be occupied by diverse magnetic or non-magnetic cations [18]. Also the M-type strontium ferrite possesses relatively large saturation magnetization, high coercive force and rather high uniaxial magnetocrystalline anisotropy, chemical stability as well as corrosion resistivity [19]. So the M-type $SrFe_{12}O_{19}$ was used as the core.

In this article, the magnetic properties of the coaxial fibers were investigated by vibrating sample magnetometer (VSM). Their photocatalytic activities were evaluated by the degradation of a model pollutant dye solution, methylene blue (MB) in a photochemical reactor. For comparison, the MB degradation over Degussa P25 was also carried out under identical conditions.

Materials and methods

Materials

Strontium(II) nitrate [$Sr(NO_3)_2$, 99.5%, A.R. Tientsin Fuchen Chemical Reagents Co] and iron(III) nitrate [$Fe(NO_3)_3{\cdot}9H_2O$, 98.5%, A.R. Tientsin Yingdaxigui Chemical Reagents Co] were used as precursors. Citric acid monohydrate ($C_6H_8O_7{\cdot}\ H_2O$, 99.5%, Tientsin Yingdaxigui Chemical Reagents Co) was used as a chelating agent. Ammonia water ($NH_3{\cdot}\ H_2O$, 25%, A.R. Tientsin Yingdaxigui Chemical Reagents Co) was used to adjust pH of the solution. Poly(vinyl pyrrolidone) (PVP, M_r = 10,000, A.R. Tientsin Damao Chemical Reagents Co) and acetic acid (CH_3COOH, A.R. 99.5%, Beijing Chemical Works) were used as a spinning aid. Tetrabutyl titanate ($Ti[O(CH_2)_3CH_3]_4$, A.R. Beijing Xingjin Chemical Plant) was chosen as a Ti resource. Distilled water and anhydrous alcohol (CH_3CH_2OH, A.R. Beijing Chemical Works), together with tetrabutyl titanate were used to coat the $SrFe_{12}O_{19}$ fibers, depositing TiO_2 coating. MB ($C_{16}H_{18}ClN_3S\ 3H_2O$) was obtained from Beijing Zhongxiyuanda Corporation to act as an organic pollutant in waste water. Degussa P25 (with 80% anatase and 20% rutile) was produced by the Degussa AG Company in Germany.

Preparation of TiO_2-coated $SrFe_{12}O_{19}$ fibers

PVP (3 g) solution (22.2 wt%) was prepared using acetic acid (10.0 mL) as solvent. The strontium ferrite precursor solution was obtained from the dissolution strontium(II) nitrate (0.25 g), iron(III) nitrate (4.99 g) and citric acid monohydrate (3.23 g), which were dissolved in distilled water (about 30 mL). The pH value (between 6 and 7) was adjusted by adding appropriate content of ammonia water to the solution. The following evaporation of water resulted in the formation of the gel. The electrospinning solution was obtained by mixing PVP solution with strontium ferrite gel (about 5 mL) under vigorous stirring for about 12 h.

The prepared electrospinning solution was loaded into a plastic tube (8–9 mm in diameter). The electrospinning process was carried out using our home-made electrospinning system. The needle was connected to a high-voltage supply, and the voltage of +18 kV was applied. The distance between the needle tip and collector was about 13.5 cm. All electrospinning processes were carried out at room temperature. The electrospun fibers were dried at 60 °C for 12 h in air. The dried fibers were calcined at 750 °C for 1.5 h in air to get strontium ferrite fibers with a heating rate of 100 °C/h.

TiO_2 coating was deposited by the tetrabutyl titanate–ethanol–ethanol/water–ethanol process [20]. $SrFe_{12}O_{19}$ fibers (0.016–0.020 g, 2–2.6 wt% of tetrabutyl titanate) were soaked in tetrabutyl titanate for 2 min with subsequent air pump filtration and rinsed 2–3 times quickly by ethanol. Then, the $SrFe_{12}O_{19}$ fibers were rinsed 2–3 times by the mixed solution of ethanol and distilled water (1:1). At last, the rinsing by ethanol was necessary. Cycles were repeated three times. The coated fibers were dried at 70 °C for 12 h in air. The dried fibers were calcined at 550–650 °C for 3 h in air to get TiO_2-coated $SrFe_{12}O_{19}$ fibers with a heating rate of 150 °C/h.

Characterization of TiO_2-coated $SrFe_{12}O_{19}$ fibers

The calcined composite nanofibers were characterized by means of X-ray diffraction (XRD) using CuKα radiation with $\lambda = 0.154056$ nm (D/MAX-IIIA, Rigaku, Japan). The micro-texture of the nanofibers was examined by scanning electron microscopy (SEM, JSM-6360LV, Japan) and transmission electron microscope (TEM, Tecnai $G^2$20 S-TWIN). The magnetic properties (coercivity H_c, specific saturation magnetization M_s, and specific remanent magnetization M_r) were performed at room temperature by VSM operating up to a maximum field of 20 kG.

Photocatalytic activity measurement

The photocatalytic activity of the TiO_2-coated $SrFe_{12}O_{19}$ fibers was evaluated by the degradation of a model pollutant dye solution, MB in a photochemical reactor, and the schematic representation of the photoreactor was shown in Fig. 1 [21]. The light was housed in the center in a quartz glass tube from the upside. The cell was at room temperature, the photocatalysis was performed at 8 °C by low temperature and constant temperature box, and the photocatalysis was kept in air.

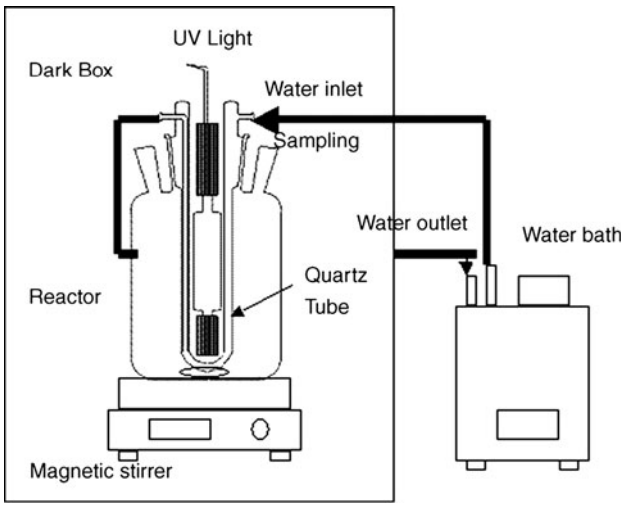

Fig. 1 Schematic representation of the photoreactor

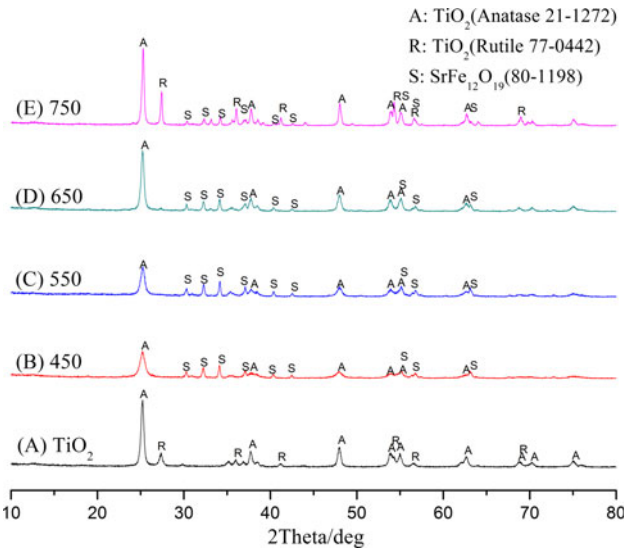

Fig. 2 XRD patterns of TiO_2 and TiO_2-coated $SrFe_{12}O_{19}$ fibers after heat treatment at 450, 550, 650, and 750 °C

First, 10 mg MB was dispersed into 400 mL deionized water. Then, 70 mg TiO_2-coated $SrFe_{12}O_{19}$ fibers were immersed into the MB solution, and the pH of the mixture was about 6.4. Before irradiation, this reaction suspension was magnetically stirred in the dark for 12 h to ensure the establishment of an adsorption/desorption equilibrium of MB on the catalyst surface before illumination. The solution was irradiated with UV light for 7 h using a 300 W high-pressure Hg lamp system (with UV light accounting for 40%, Shanghai Bilon Instruments Co, Ltd). At a given irradiation time interval (1 h), 3-mL aliquots was collected and centrifuged to remove the solid catalyst fibers. The absorbance of solution at 660 nm was measured to determine the concentration of MB using an UV–vis spectrophotometer (TU-1901, Beijing Purkinje General Instrument Co, Ltd) over the wavelength range, 190–800 nm. The equation degradation rate $(D) = [(A_0 - A)/A_0] \times 100\% = [(C_0 - C)/C_0] \times 100\%$ was used to fit experimental data, where A is the absorbance of MB solution after degradation, A_0 is the initial absorbance of MB solution before degradation, C is the solution-phase concentration of MB, and C_0 is the initial concentration at $t = 0$.

Results and discussion

Structural characteristic of TiO_2-coated $SrFe_{12}O_{19}$ fibers

X-ray diffraction patterns for TiO_2 fibers and TiO_2-coated $SrFe_{12}O_{19}$ fibers at various temperatures (450, 550, 650, and 750 °C) are shown in Fig. 2. All of the main characteristic peaks are indexed as the anatase TiO_2 (PDF Card #21-1272), rutile TiO_2 (PDF Card #77-0442), and hexagonal $SrFe_{12}O_{19}$ in the standard data (PDF Card #80-1198).

As shown in Fig. 2a, the XRD pattern of anatase TiO_2 fibers shows main diffraction peaks at 25.2° and 48.0°. Also, the sample has a rutile phase at $2\theta = 27.4°$ when the calcination temperature is 550 °C. Therefore, the fibers can be concluded to have both anatase phase and rutile phase with tetragonal structure.

Figure 2b, c, and d shows XRD patterns of TiO_2-coated $SrFe_{12}O_{19}$ fibers after heat treatment at 450, 550, and 650 °C, presenting the characteristic peaks signed A and S of anatase TiO_2 and hexagonal $SrFe_{12}O_{19}$, respectively. However, the characteristic peaks of rutile TiO_2 are not presented obviously. It is clear that the relative intensity of the characteristic peaks signed A is different from each other at different heat treatment temperatures. When the temperature of heat treatment is increased to 750 °C (Fig. 2d), the peaks corresponding to the rutile phase appear, whereas those indicating the anatase phase do not attenuate. This clearly indicates the transformation from the anatase to the rutile phase.

Figure 3a shows the SEM image of electrospun TiO_2-coated $SrFe_{12}O_{19}$ fibers. The fibers are short and relatively dense after heat treatment with a random orientation over the substrate, and the coating process made the fiber surface uneven. The failure phenomenon of the fibers after being calcined could be also observed obviously, due to a second calcination process. Figure 3b gives the TEM photograph of the TiO_2-coated $SrFe_{12}O_{19}$ fibers. It demonstrates that the fiber is composed of two kinds of substances with different contrast, and the surface is rough. As $SrFe_{12}O_{19}$ is a magnetic material, the absorption capacity of electron is much larger than TiO_2. Therefore, the dark

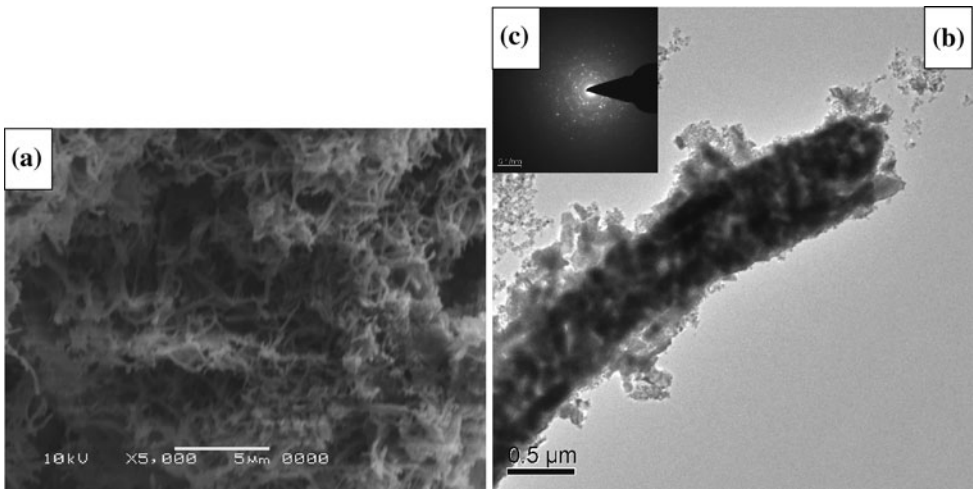

Fig. 3 SEM and TEM images of TiO_2-coated $SrFe_{12}O_{19}$ fibers

Table 1 VSM datas for different samples

	Coercivity H_c/G	Remanent magnetization M_r/(emu/g)	Saturation magnetization M_s/(emu/g)
Pure $SrFe_{12}O_{19}$	5344.3	25.761	48.197
$TiO_2/SrFe_{12}O_{19}$	5149.7	4.235	7.968

part in the core layer is $SrFe_{12}O_{19}$, and the light part in the coating layer is TiO_2 [22]. And it shows that the average diameter of the fibers is 500–600 nm. Electron diffraction pattern (Fig. 3c) displays discontinuous diffraction rings. It is confirmed that this TiO_2-coated $SrFe_{12}O_{19}$ fiber is polycrystalline.

Magnetic properties of TiO_2-coated $SrFe_{12}O_{19}$ fibers

The magnetic properties of $SrFe_{12}O_{19}$ fibers and TiO_2-coated $SrFe_{12}O_{19}$ fibers were measured by VSM, performed at room temperature. The values of the coercivity (H_c), the saturation magnetization (M_s), and the specific remanent magnetization (M_r) are summarized in Table 1.

Results reveal that TiO_2 coating affected greatly the magnetic properties of $SrFe_{12}O_{19}$ fibers. Due to the presence of a non-magnetic TiO_2 coating, the M_s and M_r values were less than that of pure $SrFe_{12}O_{19}$. This result is attributed mainly to the contribution of the concentration of the non-magnetic materials to the total sample volume [23]. Lower $SrFe_{12}O_{19}$ concentration produces lower saturated magnetization [23]. Coercivity is an important parameter of magnetic materials to reflect the degree of permanent magnetism. According to the results, the values of coercivity were nearly the same. This indicates the degree of permanent magnetism of the TiO_2-coated $SrFe_{12}O_{19}$ fibers is not heavily affected by the presence of non-magnetic TiO_2. Therefore, the samples can be separated easily in a suspended system. Moreover, the fibers can be redispersed after being separated by an external magnetic field because of their low M_r values [24].

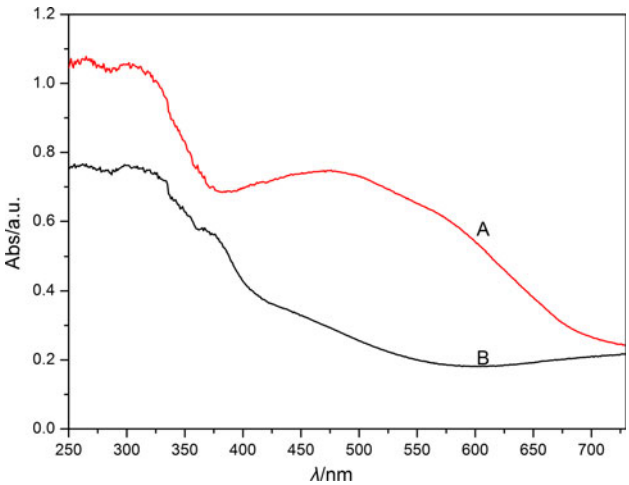

Fig. 4 The UV–vis diffuse reflectance spectra of *A* TiO_2-coated $SrFe_{12}O_{19}$ and *B* pure TiO_2 fibers

Photocatalytic properties of TiO_2-coated $SrFe_{12}O_{19}$ fibers

Figure 4 gives the UV–vis diffuse reflectance spectra of TiO_2-coated $SrFe_{12}O_{19}$ and pure TiO_2 fibers. According to Fig. 4, in contrast to pure TiO_2 fibers, the TiO_2-coated $SrFe_{12}O_{19}$ fibers have higher absorption in 250–750 nm wavelength regions. Anatase TiO_2 only has absorption peaks in 250–400 nm wavelength regions. Therefore, only UV illumination of TiO_2 can excite electrons from the valence band to the conduction band, leaving holes in the valence band. Then, the electrons react with oxygen to produce superoxide anions (O_2^-), and the holes react with water to produce hydroxyl radicals (OH). These two species are very reactive, and able to decompose a variety of organic toxic chemicals in water [25]. The TiO_2-coated

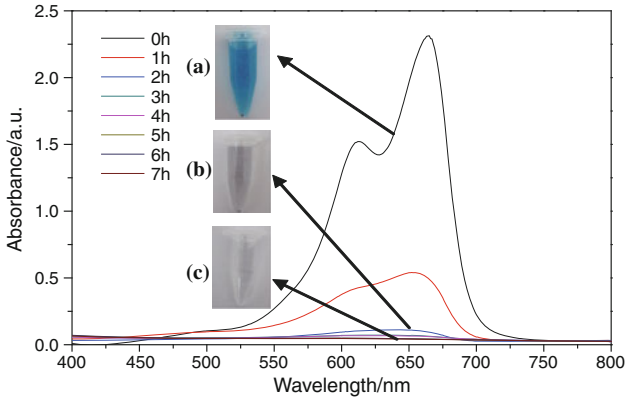

Fig. 5 UV–vis absorbance of MB solution containing TiO_2/$SrFe_{12}O_{19}$ fibers as a function of the irradiation time: **a** 0 h, **b** 2 h, and **c** more than 3 h

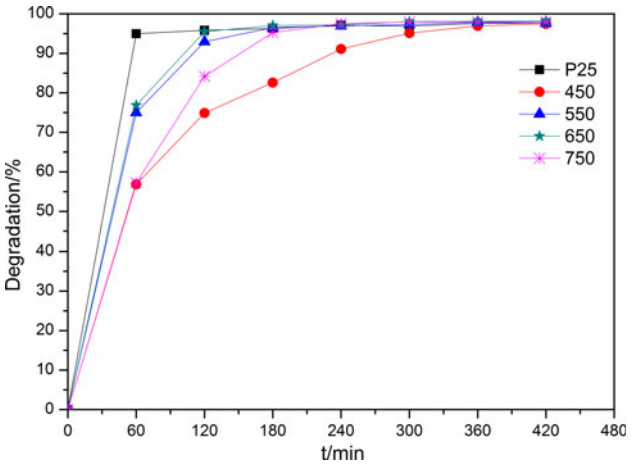

Fig. 6 Effect of the calcining temperature of TiO_2-coated $SrFe_{12}O_{19}$ fibers on decolorizing efficiency of MB under UV irradiation and photocatalytic activity of P25

$SrFe_{12}O_{19}$ generates red shift, and also has higher absorption in visible region (400–700 nm).

Figure 5 reveals the change in the absorbance on the UV–vis spectrum of the MB solution containing TiO_2-coated $SrFe_{12}O_{19}$ fibers as a function of the UV irradiation time up to 7 h.

The mechanism of the photocatalytic reaction in the presence of TiO_2 involves a free-radical reaction that is initiated by UV light [26]. The photocatalytic activity of TiO_2 strongly depends on the crystalline phase and surface area [26]. The photocatalytic degradation of the MB solution was used as a model photoreaction, and the photocatalytic activity was measured from the UV–vis absorbance at 660 nm, which is the maximum absorbance peak of MB in solution [1, 27, 28]. As the photodegradation of the MB solution proceeded, the absorbance on the UV–vis spectrum decreased gradually, which can be seen obviously from the vanishing blue color. The blue color has nearly vanished after 3-h irradiation. The decrease in absorbance is probably due to degradation of the MB chromophore [29], and the concentration of MB decreased gradually. Therefore, the intensity of the absorbance is proportional to the concentration of MB in the solution at 660 nm. So this wavelength has been chosen to determine the rate of degradation reaction by measuring the intensity of the absorbance of the MB solution.

Figure 6 shows the effect of TiO_2-coated $SrFe_{12}O_{19}$ fibers at different calcining temperatures on decolorizing efficiency of MB under UV–vis irradiation. The rates of MB degradation are different with increasing the calcining temperature of TiO_2-coated $SrFe_{12}O_{19}$ fibers from 450 to 750 °C, but nearly all of the decolorizing efficiency were up to about 98% in 7 h. Under relatively low calcining temperature, the anatase crystalline structure of TiO_2 is imperfect. With increasing the calcining temperature, the crystal of TiO_2 grows up gradually. However, when up to certain temperature (750 °C), it has led to polymorphic transition of titanium dioxide from anatase to rutile. The rutile TiO_2 has lower photocatalytic efficiency than anatase TiO_2, so it will partly decrease the decolorizing efficiency. Meanwhile, the rate of the MB decomposition (97.7%) over Degussa P25, which is known as the best photocatalyst commercially available, is a little lower than the decomposition over TiO_2-coated $SrFe_{12}O_{19}$ fibers (98.2%) in 7 h.

Separable ability

Figure 7 shows that the TiO_2-coated $SrFe_{12}O_{19}$ fibers were separated from the MB solution by a strong permanent magnet. The process of magnetic separation was obvious. In Fig. 7a, the water was rather feculent, but in Fig. 7b, the

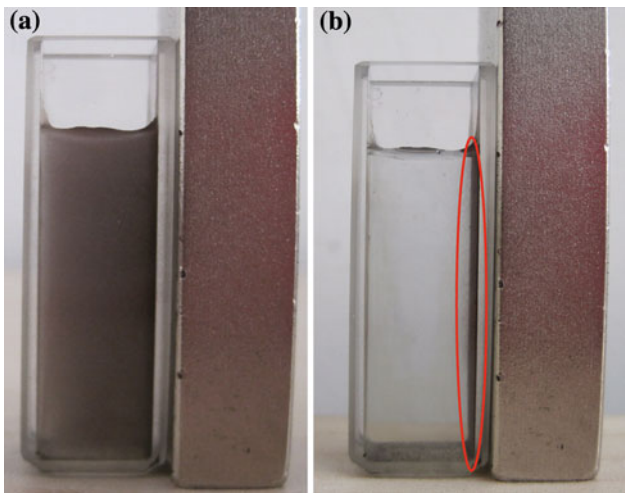

Fig. 7 Magnetic photocatalyst fibers were separated from a solution by a strong permanent magnet (*right*)

water became lighter. The separated fibers were on the right, where a strong permanent magnet was. By this approach, we have successfully reached our goal of efficient recycling of the magnetic photocatalyst.

Conclusions

In conclusion, the magnetic photocatalysts, TiO_2-coated $SrFe_{12}O_{19}$ fibers, were successfully fabricated by combining electrospinning, sol–gel, and coating technology. The average diameter of the electrospun fibers was 500–600 nm. The decolorizing efficiency of MB under UV–vis irradiation was up to about 98.2%. These fibers can be recollected easily with a magnet from the solution in a photocatalytic process.

Acknowledgement This study was partly supported by the Natural Science Foundation of China (Grant no. 51073005), the Beijing Natural Science Foundation (Grant no. KZ201010012012), PHR (IHLB), the 863 Project (Grant no. 2007AA021906), and the 973 Project (Grant no. 2010CB933501).

References

1. Alves AK, Berutti FA, Clemens FJ, Graule T, Bergmann CP (2009) Mater Res Bull 44:312
2. Zhang BP, Zhang JL, Chen F (2008) Res Chem Intermed 34:375
3. Kim S, Lim SK (2008) Appl Catal B Environ 84:16
4. Ao YH, Xu JJ, Fu DG, Yuan CW (2009) J Alloys Compd 471:33
5. Kanjwal MA, Barakat NAM, Sheikh FA et al (2010) J Mater Sci 45:1272. doi:10.1007/s10853-009-4078-3
6. Hu GJ, Meng XF, Feng XY et al (2007) J Mater Sci 42:7162. doi:10.1007/s10853-007-1609-7
7. Santala E, Kemell M, Leskelä M, Ritala M (2009) Nanotechnology 20:035602
8. Dong SH, Xu KJ, Tian GS (2009) J Mater Sci 44:2548. doi:10.1007/s10853-009-3332-z
9. Formo E, Lee E, Campbell D, Xia YN (2008) Nano Lett 8:668
10. Li D, Xia Y (2004) Adv Mater 16:1151
11. Reneker DH, Chun I (1996) Nanotechnology 7:216
12. Frenot A, Chronakis IS (2003) Curr Opin Colloid Interface Sci 8:64
13. Huang ZM, Zhang YZ, Kotaki M, Ramakrishna S (2003) Compos Sci Technol 63:2223
14. Subbiah T, Bhat GS, Tock RW, Pararneswaran S, Ramkumar SS (2005) J Appl Polym Sci 96:557
15. Li D, McCann JT, Xia Y (2006) J Am Ceram Soc 89:1861
16. Guo YZ, Li CJ, Wang JN (2009) Chin J Inorg Chem 25:1018
17. Li CJ, Wang JN (2010) Mater Lett 64:586
18. Nga TTV, Hien TD, Duong NP, Hoang TD (2008) J Korean Phys Soc 52:1474
19. Nga TTV, Duong NP, Hien TD (2009) J Alloys Compd 475:55
20. Chu JY, Yu Q, Wu CD, Cao CL, Li N (2008) J Inorg Mater 23:652
21. Zuo XW, Fei P, Hu CL, Su BT, Lei ZQ (2009) Chin J Inorg Chem 25:1233
22. Wan MX, Li WG (1997) J Polym Sci Polym Chem 35:2129
23. Chiou CH, Wu CY, Juang RS (2008) Chem Eng J 139:322
24. Ao YH, Xu JJ, Zhang SH, Fu DG (2009) J Phys Chem Solids 70:1042
25. Lee JA, Krogman KC, Ma M, Hill RM, Hammond PT, Rutledge GC (2009) Adv Mater 21:1252
26. Kim YB, Cho D, Park WH (2010) J Appl Polym Sci 116:449
27. Zhan S, Chen D, Jiao X, Song Y (2007) Chem Commun 20:2043
28. Zhang T, Ge L, Wang X, Gu Z (2008) Polymer 49:2898
29. Rizzo L, Koch J, Belgiorno V, Anderson MA (2007) Desalination 211:1